Chapter 2
Heterogeneity in Crosslinked Polymer Networks: Molecular Dynamics Simulations

D.M. Kroll and S.G. Croll

Introduction

Crosslinked network polymers are a widely used class of chemicals and have been utilized since people used any form of paint, e.g., with proteins (casein, tempura) or unsaturated vegetable oils. Modern high-performance technology relies on different chemistry, such as epoxies, polyurethanes, and rubbers, but the continual search for improvements relies on increasing our understanding of how two or more reactive precursors form the desired network. When these modern technologies were first implemented, considerable advancements could be made rapidly; more recently however, as with all mature technologies, further progress is much more difficult and requires a greater degree of insight. Networks are formed from small molecules that react with other small molecules, and the resulting network topology depends on the specific interactions (chemistry) and the distribution and availability of these precursors, which is governed by their random location and motion. Thus, it is reasonable to expect that one can describe the resulting networks using statistical approaches which have been very successful at describing how representative molecular properties affect macroscopic network properties [1–4].

A simple calculation provides some perspective. We might consider a coating has failed when the density of visible features such as rust spots and blisters reaches a concentration of 1 per square centimeter. A polymer coating 1 cm^2 in area might have a typical thickness of 50 μm and thus a volume of $5 \times 10^{+21}$ $Å^3$. If we approximate the volume of most atoms as 1 $Å^3$, it is easy to appreciate that, while

D.M. Kroll
Department of Physics, North Dakota State University, Fargo, ND, USA

S.G. Croll (✉)
Department of Coatings and Polymeric Materials, North Dakota State University, Fargo, ND, USA
e-mail: Stuart.Croll@ndsu.edu

M. Wen, K. Dušek (eds.), *Protective Coatings*, DOI 10.1007/978-3-319-51627-1_2

most crosslinking reactions will proceed as anticipated, there is a chance that an appreciable number will not, at random, and will lead to a variety of heterogeneities. As long appreciated [1, 5, 6], as a crosslinking system proceeds toward its gel point, the various partially crosslinked components become much less able to move, and thus the reactive species cannot mix and react homogeneously. Heterogeneities can take the form of unreacted functionalities, dangling ends and chains that return to the same network junction and thus form loops. Since the numbers involved are so large, one can imagine several such occurrences in a neighborhood contributing to a more extended region of inconsistent crosslinking.

Although they are a natural consequence of the large numbers of entities involved in the crosslinking process, these heterogeneities inevitably detract from the performance of the network and will therefore be referred to here as imperfections, flaws, or defects. Polymer coatings are most often used to protect something or improve its appearance. Protective requirements can be diverse, but they often rely either on the mechanical properties of the crosslinked polymer or its ability to prevent aggressive chemicals from reaching the underlying engineering material, e.g., metals that may corrode. Network imperfections force the gelation point to occur at a higher value of chemical conversion than anticipated and may limit the toughness and mechanical strength or enable water, salts, or other chemicals to permeate too easily. Adhesive joints may fail, rust spots appear at unplanned places on a painted metal part, and caulks and sealants may spring a leak, seemingly at random places. Exposure to aggressive environments leads to chemical and physical degradation and thus failure. The quality of the starting material determines, at least in part, its success in service, so heterogeneities that arise during the network formation may be crucial.

Information on heterogeneities and imperfections, at the molecular level, is generally difficult [7], if not impossible, to obtain experimentally. In molecular dynamics simulations, however, molecular architecture and the crosslinking reactions can be specified, and a detailed picture of network structure and its heterogeneities can be determined. Modern computers and software enable us to investigate large system sizes and create crosslinked systems in which the location and connections of every molecule or bond are tabulated. For example, Duering et al. [8, 9] studied tetrafunctional networks with strand lengths ranging from 12 to 100 monomers and compared their results to the predictions of the rubber elasticity theories. Here, we also use coarse-grained molecular dynamics to investigate highly crosslinked networks typical of high-performance coatings, as distinct from rubbery materials which may have almost an order of magnitude lower crosslink density. The systems studied here prove to have heterogeneities that range from small, molecular size defects to features that extend across the whole simulated volume.

Background

For ideal networks, the statistical theories of Flory and others [1, 2, 10, 11] are very successful and provide algebraic equations that have been used for many decades to describe the rubbery elastic, mechanical properties in terms of a characteristic

length of the network chains between crosslinks, their concentration, and the number of reactive functionalities at the network junctions. This approach was extended [12] to describe the ability of a solvent to swell a crosslinked polymer by including the Flory–Huggins theory for miscibility. A later approach recognized that gelation could be modeled as a process on a Bethe lattice [13, 14] and gave results supporting the findings of the statistical models. Others, notably Dušek [15–17] and Miller and Macosko [18, 19], used kinetic and recursive equations to calculate the likely crosslink chain length and density from the structure of the reactive precursors and thus enabled the prediction of macroscopic properties using the statistical models for rubber elasticity. Unless there is a specific effort to model the formation of loops [20], the recursive approach, like the Bethe lattice approach, is known to model dendritic structures, not networks [21]. However, these approaches are well known and successful for calculating the expected, average properties of a rubbery network, but they have no means of estimating the number and extent of heterogeneities, although one can compare predictions with experiment and, for example, deduce a ring-forming parameter [6] that accounts for the discrepancy.

Early in the development of these statistical models, it was realized that unreacted chain ends and other imperfections must be accounted for [1] and that spatial neighbors may not be joined by chemical bonds [22]. Reflecting the fact that only elastically active chains contribute, Flory proposed the cycle rank to calculate the mechanical properties of the network. In the so-called phantom network approach, the shear modulus of the rubbery material, G_{ph}, is proportional to the cycle rank, ξ, which is the number of complete loops in the network:

$$G_{\mathrm{ph}} = \xi k_{\mathrm{B}} T / V \tag{2.1}$$

where T = temperature, V is the volume of the system, and k_{B} is Boltzmann's constant.

The simpler "affine" model for rubber elasticity assumes that all network chains are elastically effective so that the modulus is

$$G_{\mathrm{aff}} = \nu_{\mathrm{e}} k_{\mathrm{B}} T / V \tag{2.2}$$

The cycle rank, ξ, is given by the difference between the number of elastically active chains, ν_{e}, and the number of elastically active junctions, μ_{e}. In a perfect network without heterogeneities, the cycle rank is simply related to the network functionality [23]:

$$\xi = \nu_{\mathrm{e}} \left(1 - \frac{2}{\phi} \right) \tag{2.3}$$

where ϕ is the functionality of the crosslink junctions (3 or 6 here). For a tetrafunctional network ξ is simply $\nu_{\mathrm{e}}/2$ [24].

The Miller–Macosko (MM) approach can be used to predict values for the chain length between crosslinks, the cycle rank, etc., from the functionality, structure, and concentration of the reactive precursors. Like the statistical theories, and the Bethe lattice approach, MM calculations have no explicit recognition that networks form loops. Their calculations assume an ideal treelike growth of the network, and the criterion for an elastically effective link is that the path through the network continues indefinitely. There is also a considerable body of work by Dušek that has examined a variety of specific combinations of reactants to calculate the characteristics of the resultant networks [16]. Molecular dynamics simulations [25] have shown the variation possible in crosslink density and the effect on the mechanical properties of rubbers of long dangling chains and varying sizes of loops. The work here uses coarse-grained molecular dynamics and examines the heterogeneities in highly crosslinked networks characteristic of high-performance coatings and rigid composites and compares results with MM calculations, since they give very useful estimates of average properties of ideal networks.

Model and Simulation Method

Molecular dynamics is a very versatile approach that could be used to examine a myriad of networks. Here we study two simple, but distinctly different, coarse-grained models to model networks similar to those produced using a wide range of chemical options. The models consist of precursors composed of a two-bead "chain extender" and a crosslinker of functionality $f = 3$ or 6. These, and similar models, have been used before [26–29] to study fracture, thermomechanical properties, and cavitation in crosslinked networks. The 6-functional network is formed with one chain extender molecule already bonded to its 6-functional crosslinker bead prior to starting the simulations, but this pre-bonding has no noticeable effect on the resulting network connectivity [29]. The 3-functional model has a crosslinker with a central 3-functional node connected to three single functional beads. Diagrams of the network structures are shown in Fig. 2.1.

The interactions used to model bead behavior and interactions are completely conventional. All beads interact via van der Waals forces modeled by a Lennard-Jones (LJ) potential, $U(r)$, which is cut off at a radius, $r_c = 2.5\sigma$, and shifted upward so that the potential is equal to zero at r_c:

$$\begin{aligned} U(r) &= U_{\mathrm{LJ}}(r) - U_{\mathrm{LJ}}(r_c) \quad \text{for } r \le r_c \\ &= 0 \qquad\qquad\qquad\qquad\quad \text{for } r > r_c \end{aligned} \tag{2.4}$$

where

$$U_{\mathrm{LJ}}(r) = 4\varepsilon\left[\left(\frac{\sigma}{r}\right)^{12} - \left(\frac{\sigma}{r}\right)^{6}\right] \tag{2.5}$$

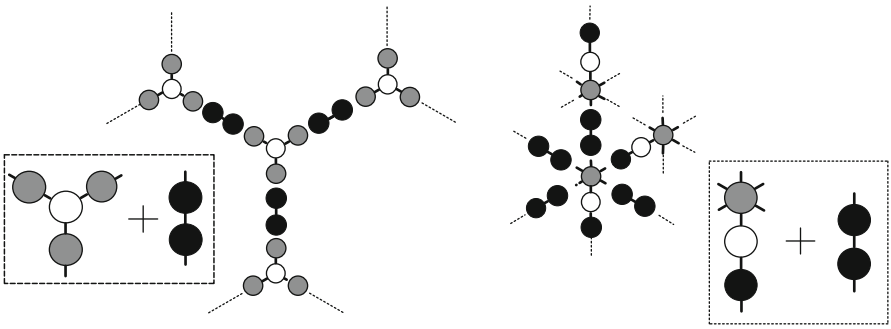

Fig. 2.1 Schematic diagrams showing the precursors, in *boxes*, and the connections for the 3-functional network (*left*) and the 6-functional network (*right*)

Here, σ is the characteristic length of the LJ potential, r is the distance between bead centers, and ε is the energy parameter for the strength of the interaction. This models van der Waals attractive forces very well and has a strong repulsive core that defines the size of the bead. Covalent bonds between beads, either preexisting or formed during crosslinking, are described by a bond potential that is the sum of the purely repulsive LJ interaction with a cutoff at $2^{1/6}\,\sigma$ (the minimum of the LJ potential) and a finite-extensible nonlinear elastic (FENE) attractive potential:

$$U_{\mathrm{FENE}}(r) = \begin{matrix} -0.5R_0^2 k \log_{\mathrm{e}}\left[1 - \left(\frac{r}{R_0}\right)^2\right] & r < R_0 \\ r = \infty & r \geq R_0 \end{matrix} \tag{2.6}$$

where the force constant, $k = 30\varepsilon/\sigma^2$, and the maximum bond length, $R_0 = 1.5\sigma$. These are commonly used parameter values [29]. The FENE bond is ~10% shorter than LJ bonds and emulates the increased density in solid crosslinked polymers with respect to the liquid precursors; it also prevents chain crossing. The MD simulations were performed using the Large-Scale Atomic/Molecular Massively Parallel Simulator (LAMMPS) [30].

Results were obtained from simulations of stoichiometric mixtures, as before [29], of crosslinkers and dimers with a total system size of 11,424 beads. Averages were taken over five independent realizations for each set of parameters. A limited number of simulations were performed for larger systems. Before crosslinking, the precursor "molecules" are given random locations and equilibrated at a high temperature, $T = 1.0\varepsilon/k_{\mathrm{B}}$, and at zero pressure using a Nosé–Hoover thermostat and barostat with a time step of 0.005τ, where $\tau = \sigma(m/\varepsilon)^{1/2}$ is the Lennard-Jones unit of time. Temperatures are given as multiples of the Lennard-Jones energy parameter with respect to Boltzmann's constant (henceforth, for convenience, the units of temperature will be omitted in the text). The networks are then dynamically crosslinked at constant temperature and zero load as before [26–29].

Two different approaches to crosslinking were taken. In the first, crosslinking was performed at several temperatures ranging from $T = 1.0$ down to $T = 0.1$ and $T =$ "0," since many coating and composite polymers are cured at a variety of temperatures, including many crosslinked systems that must be cured and used at ambient temperatures, e.g., epoxy adhesives and coatings, polyurethanes, and alkyd paints. Here, $T =$ "0" corresponds to the complete elimination of thermal fluctuations and therefore does not correspond to a situation attainable in the laboratory or applications. Nonetheless, it is an interesting limit because it provides insight into the influence of diffusion in network formation. In this case, crosslinking consisted of successive crosslinking and energy relaxation iterations until the same number of crosslinking attempts were performed as at finite temperature. The crosslinking procedure was the same as that applied at finite temperature [26–29]. The energy relaxation steps allowed the systems to relax to its lowest energy state as crosslinking proceeded. Results in this case were found to be very similar to those obtained when crosslinking at $T = 0.1$. Furthermore, percolating networks were also obtained in this case (without diffusion), indicating that the precursor solution was sufficiently randomized so that typical crosslinkers were surrounded by a sufficient number of active sites for crosslinking to proceed beyond the gel point. The pre-gel cluster growth process was found to be consistent with the predictions of percolation theory.

The 3-functional system was crosslinked for twelve million time steps and the 6-functional system for six million time steps. Networks crosslinked at high temperatures had properties consistent with what is observed with actual crosslinking polymers, which are frequently cured above their eventual glass transition temperature to ensure a high and stable degree of conversion in a reasonably short manufacturing process. Below T_g, crosslinking proceeded more slowly, resulting in lower conversions [31, 32]. Coating systems seldom cure completely; in these simulations, as in practice, conversion was continued until it was varying only very slowly and was characteristic of the conditions [31, 32].

Having determined these characteristic conversions, crosslinked networks with the same range of conversions were also made by crosslinking at the highest temperature, $T = 1.0$, at which all the components have a high degree of mobility. This is a very common and simple approach in computational simulations and provides another curing regime that can lead to insights on how network quality depends on the curing schedule.

A network search algorithm was developed [24, 25, 33] to determine the number of elastically active junctions, μ_e (a crosslink site that is connected by at least three paths to the gel), the number of elastically active chains, ν_e (an active chain is terminated by active junctions on both its ends), and the number of elastically active beads, as well as other quantities such as the number of dangling chains and primary loops. First, we identify the largest cluster (the backbone or gel) which forms the network, using a "depth first" search. Then, the backbone is searched using a "burning" algorithm [33] to examine the connectivity of junctions, i.e., if they connect to the gel, form a loop or end without connecting to the gel. Only those

links which are connected by three paths to the gel are active junctions, and the number of bonds between them is the length of the active strands.

Prior work on these systems has shown that there are portions of the crosslinked network that are sufficiently heterogeneous to permit cavitation of regions much larger than the typical bond length in the network [29]. In order for this to occur, a sufficiently large number of nodes in close spatial proximity before cavitation must be distant neighbors along the network backbone, since the network bonds are essentially inextensional, and nodes near the surface of the cavitating region must be free to move apart to form the void. One of the advantages of molecular dynamics simulations is that the characterization of the network, topological defects, and pore space created under various conditions such as swelling can be studied in detail. We have used molecular dynamics simulations to analyze these topological defects and have found that their presence results in networks in which the number of elastically active chains, the cycle rank, and the number of elastically active junctions are smaller than predicted by the Miller–Macosko theory [34]. This effect is particularly pronounced in the high functionality, $f = 6$, model, where crosslinking at high temperatures leads to a large number of primary loops. Such defects adversely affect the mechanical properties, resistance to solvent swelling, and, possibly, the long-term protective properties of polymer networks.

Defects can be better seen if the network density is reduced. To that end, after the networks have been formed they are allowed to expand by removing the attractive part of the LJ interactions. While the bonding potentials along the network backbone provide network integrity, it is the attractive tails of the nonbonded Lennard-Jones interactions that maintain the system in the high-density condensed state. By replacing these interactions with a purely repulsive potential obtained by cutting of the LJ potential at its minimum and shifting it upward so that the potential is zero at the cutoff, thermal fluctuations will cause the networks to swell until the fluctuation-induced entropic forces are balanced by the network restoring forces. The strength of the entropic repulsion is proportional to T, so that its strength can be tuned if desired. Here, however, it is used simply to swell the network so that the resulting voids and network structure can be visualized and analyzed more readily.

Heterogeneities in Network Polymers

Although the interest here is on observing and quantifying the heterogeneities that occur in simulations of crosslinked network, it is useful to understand some basics of how they arise.

Figure 2.2 shows the temperature–density, T–ρ, phase diagram of pure LJ systems. Since the only attractive nonbonded forces in the system are provided by the LJ interactions, it is shown here to provide some perspective for interpreting the results. It is important to remember, however, that this is not the phase diagram of the precursor solutions or the bonded networks. The thick black curve (3-functional) and thick grey curve (6-functional) show the trajectory of the

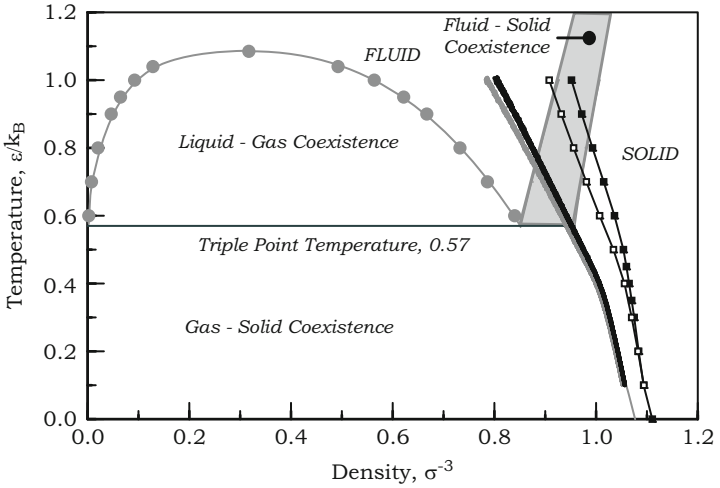

Fig. 2.2 Phase diagram of the cutoff, shifted Lennard-Jones fluid. The *grey bullets* mark the gas–liquid coexistence curve obtained from Gibbs ensemble simulations performed using the MCCCS Towhee simulation package [35]. The critical point estimate is taken from [36]. The *shaded region* is the liquid–solid coexistence region obtained using the procedure described in [37, 38]. The *horizontal grey line* is located at the triple-point temperature. The *grey* (6-functional) and *black* (3-functional) *lines* are the constant pressure ($P = 0$) trajectory of the precursor solution as it is cooled slowly from $T = 1$ to $T = 0.1$. *Squares* are data for the density after crosslinking at that temperature for the 3-functional system (*open squares*) and for the 6-functional system (*filled squares*)

precursor solutions as they are cooled at zero load at a rate of $4 \times 10^{-5}\tau^{-1}$ from $T = 1$ to $T = 0.1$. The high-temperature portion of the trajectories, for $T \geq 0.72$, is in the single phase, fluid region; at lower temperatures, they cross into the two-phase liquid–solid portion of the phase diagram before following the gas–solid coexistence line as the temperature diminishes toward zero.

Because of the comparatively short FENE bond length, the density of the system increases during crosslinking, as it does in practice when a solid polymer forms from the liquid reactants. The squares in Fig. 2.1 show the density of the crosslinked systems, and the change in slope indicates the location of the glass transition temperature, which is always in the solid part of the phase diagram. Rapid diffusion should play a large role during the initial crosslinking process for systems at $T \geq 0.8$ since the reacting system is fluid or in the solid–fluid coexistence region. Systems crosslinked at lower temperatures will almost immediately become solid, so large-scale diffusion will become difficult and one can expect that the structure of the resulting networks will depend on the crosslinking temperature. Many of the topological differences discussed later, if they occur early, must remain after gelation since subsequent changes happen only slowly and, in any case, crosslinking entails very strong bonds that inhibit significant movement away from the spatial arrangement at the point when the node is crosslinked.

Local-Scale Heterogeneities

Crosslinking reactions cannot occur uniformly because large molecules of reacted matter cannot diffuse rapidly. Sooner or later, molecules become much less mobile and can only react with their neighbors. Thus, an unreacted end might remain unreacted when opportunities around it are depleted or it reacts with the crosslink junction where its other end is attached, so a loop forms. In this way, the network can gain defects whose size is of the order of a coarse-grained bead or larger. Thus, depending on the defect concentration, one can appreciate that water or a corrosive ion would find it much easier to penetrate and cause harm in their neighborhood.

Figure 2.3 shows that a highly functional network, especially if it is cured rapidly at a high temperature, has many loops and an appreciable concentration of unreacted pendant network strands. A 6-functional network may have as many as 75% of the network junctions with a loop attached, or a 10% chance of a dangling end, and thus have a high probability of a defect in their neighborhood and a lower effective functionality. The redeeming feature of a 6-functional junction is that it probably has four other reactive sites for inclusion in a network even if two are occupied by a loop. The results for the 3-functional network are not so striking but, depending on the degree of conversion, may have almost 10% of its junctions with a loop. A 3-functional junction with a loop cannot be useful network junction; it is connected to the network through one functionality only and must form a pendant. The defect labelled here as a "dangling chain" is one with an unreacted site on the final bead, which is a different form of defect. All these defects are equivalent to a few beads in size and are local in extent, see Fig. 2.4. These defects diminish the number of elastically active loops in the network and lead to the use of cycle rank to quantify the strength of a network, rather than simply the crosslink chain density.

The illustrations in Fig. 2.4 visualize the results given in Fig. 2.3. They show that networks crosslinked at high temperature have a larger number of primary loops but comparatively few dangling or unreacted ends. The enhanced diffusion at high temperatures makes it possible for primary loops to close. In contrast, networks crosslinked at low temperatures have relatively few primary loops but many dangling and unreacted ends. Illustrations for the 6-functional network are very dense, but the differences are apparent. Loops and dangling ends reduce the effective functionality of the network. Figure 2.5 shows how that changes with the degree of conversion in both the 3-functional and 6-functional systems. Here, the effective functionality is calculated using

$$f_{\text{eff}} = [\text{bonds made}] - 2 \times [\text{primary loops}] - [\text{dangling chains}] \tag{2.7}$$

f_{eff} is the number of bonds of a crosslink junction leading to a neighboring crosslink site and is given as a fraction of the nominal functionality in each system.

These localized defects have consequences not only in the likely permeability but also in the macroscopic properties. Equations 2.1 and 2.2 are predictions of familiar theories that express the modulus of a rubbery network in terms of either

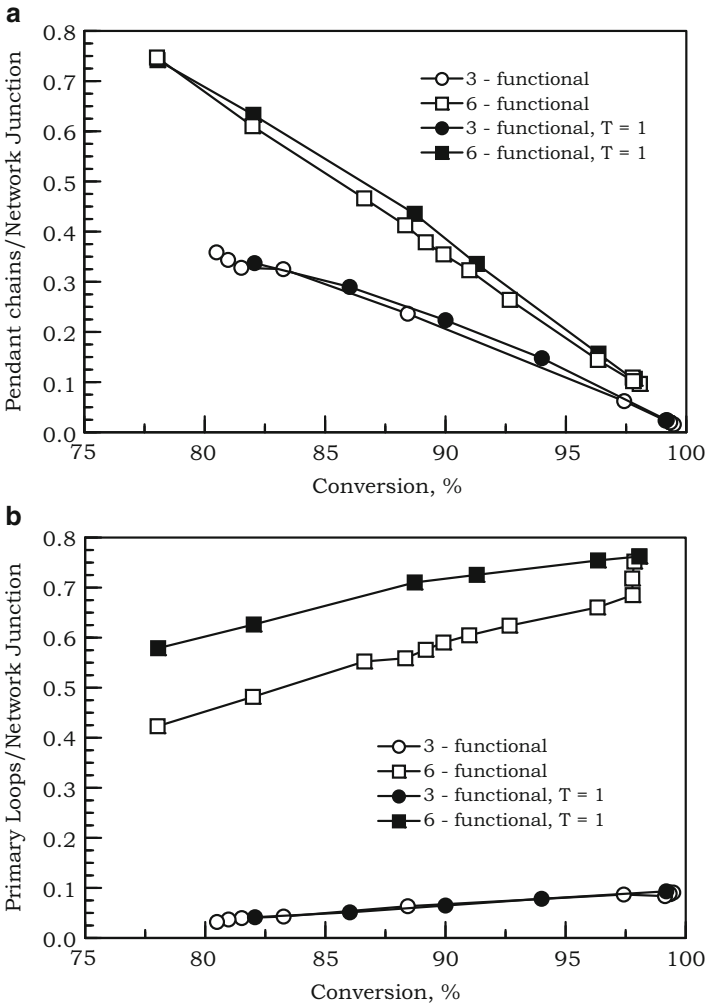

Fig. 2.3 The number of (**a**) dangling chains and (**b**) loops per network junction on the gel backbone as a function of the conversion of the 3- or 6-functional system. *Open symbols* are for systems crosslinked at different temperatures; *filled symbols* are results for crosslinking at $T = 1.0$ to a range of conversions

the cycle rank or the number of elastically active chains. Figure 2.6 provides a comparison of simulation results for the number of elastically active chains and nodes and the cycle rank with the predictions of the Miller–Macosko theory.

The MM approach makes the same ideal network assumptions as Flory, i.e., that all functional groups of the same type are equally reactive; all groups react independently of one another, and no intramolecular reactions occur in finite species.

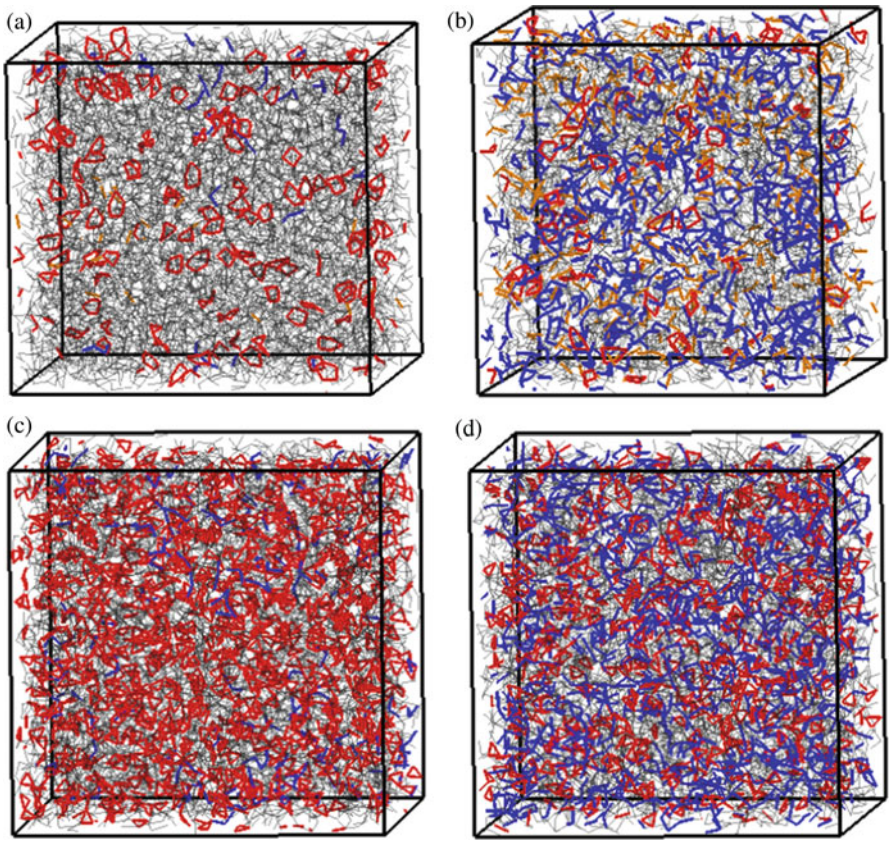

Fig. 2.4 Networks generated at $T = 1$ (*left*) and $T = 0.1$ (*right*). The network backbone bonds are shown in *black*; primary loops are *red*, dangling ends *blue*, and unreacted junction ends are *orange*. (**a**) 3-functional, $T = 1.0$, (**b**) 3-functional, $T = 0.1$, (**c**) 6-functional, $T = 1.0$, (**d**) 6-functional, $T = 0.1$

As can be seen in the figure, all quantities are diminished by approximately 20% for the 3-functional system regardless of conversion. However, for this system, the ratio between cycle rank and number of crosslink chains (Eq. 2.3) remains very close to that for the ideal network. Nevertheless, the modulus will be only approximately 80% of the expected value and, for analogous reasons, the network will swell more than an ideal network in the presence of a suitable solvent. The situation for the 6-functional system is more complex, and its performance relative to an ideal network will be worse. In this case, the number of elastically active crosslink chains is approximately 70% of the value predicted for an ideal network, and the cycle rank is 56% of that predicted for an ideal network, at high conversion. Even though cycle rank is used to describe the properties of a network in terms of the number of complete loops, and thus discount ineffective chains and junctions, any value predicted from statistical models is likely to be an overestimate.

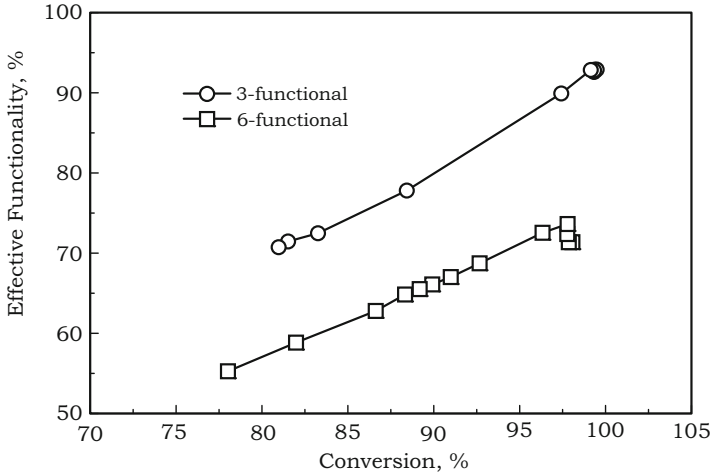

Fig. 2.5 Effective functionality of the 3- and 6-functional systems, quantifying how the functionality is reduced to a fraction of its nominal value by the imperfections

These localized defects, which are a natural consequence of the random processes of the curing of a huge number of molecules, in any system, provide a substantial number of places in the network where a penetrant molecule might more easily rest or pass through as well as reduce the stiffness and resistance to overall swelling.

So far the discussion has treated these defects as individual, perhaps isolated, features although there seems to be a high-enough concentration that they must provide some possibility of a defect pathway percolating through a network. The discussion now looks at how these defects might be organized into larger-scale features.

Extended Heterogeneities

Randomness intrinsic to the crosslinking process also leads to large-scale heterogeneities in network topology reflected by the fact that a significant number of nodes in close spatial proximity are only distant neighbors along the network backbone. This property, which is not shared by homogeneous, ideal, networks with uniform crosslinking, can be quantified in terms of the distribution of the length of the shortest path (along the network) between spatial nearest neighbors, determined by a Voronoi construction. Figure 2.7 shows the resulting distribution functions for networks crosslinked at $T = 1.0$ to conversions greater than 0.98. The number of paths is on a logarithmic axis, so one can see that the large majority of spatial neighbors are more or less directly connected, but there are significant tails

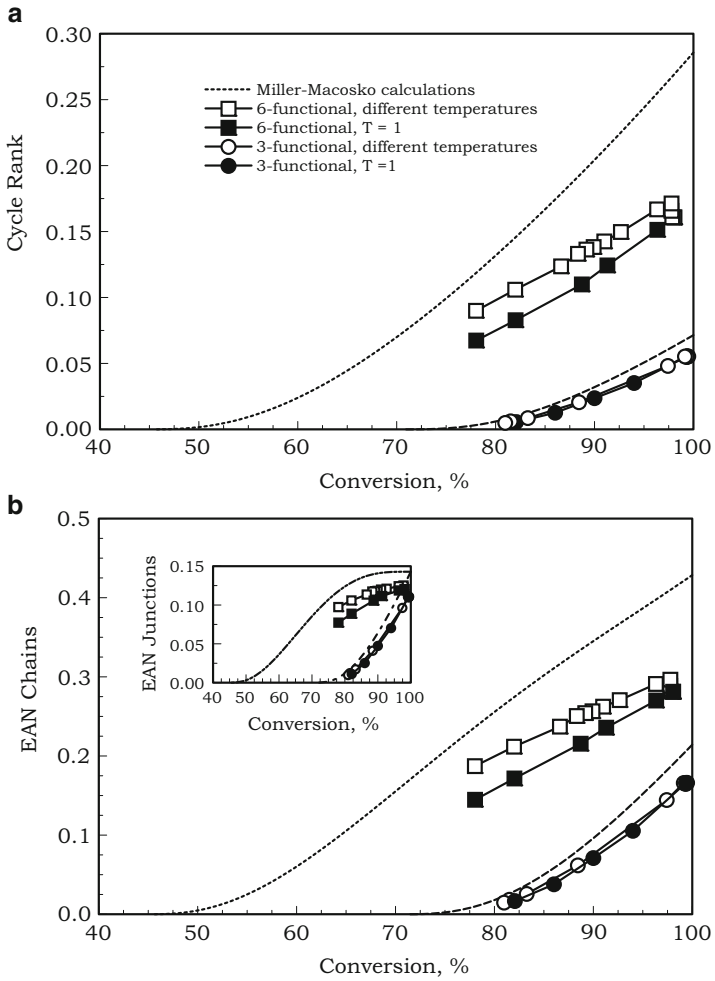

Fig. 2.6 Comparison of results from simulations with Miller–Macosko calculations (*dashed lines*) for the cycle rank (**a**), number of elastically active network chains and number of elastically active network junctions (**b**), for 3- and 6-functional systems. All network parameters are given as a fraction denominated by the total number of beads used in the simulation. The single legend is applicable to all the data

in the distributions. The much longer tail in the distribution for the 3-functional model is, in part, due to the fact that the shortest path between neighboring junctions is three bond lengths in the 6-functional model but five bond lengths in the 3-functional model.

There are more paths from a 6-functional junction that can be linked to the next, so if a crosslinked junction has a loop or pendant chain occupying one or more of

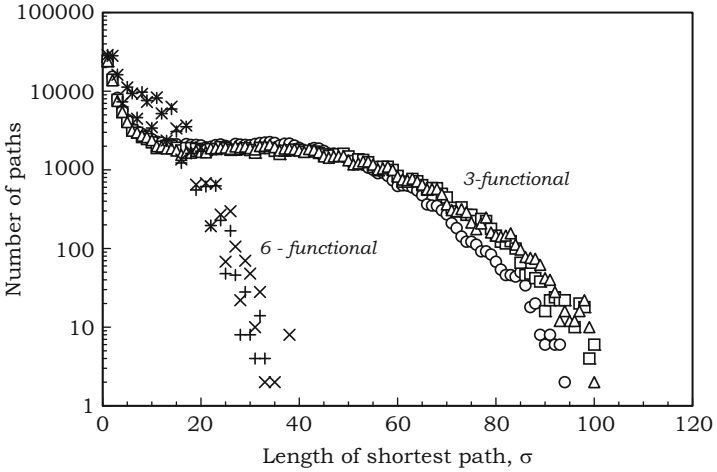

Fig. 2.7 Number distribution for the length of the shortest path, in terms of the number of bonds that must be travelled from one bead before arriving at a spatially neighboring bead. Networks crosslinked at $T = 1$ (conversion > 0.98). The *different symbols* indicate some of the (5) replicate simulations

the functionalities, there is still a good chance that it may be linked to the neighboring bead. On the other hand, a 3-functional junction has much reduced opportunities to be linked to the next bead if it also has a pendant or loop.

Some insight into the origin of these extended heterogeneities can be obtained by considering how the crosslinked clusters grow before gelation. Initially, each reactive group will find its co-reactant and form a larger molecule, but as the conversion progresses, some molecules will become larger than others, and when two growing molecules react together, they become a much larger molecule. The result is that the growing network forms clusters of reacted material in a way that is similar to diffusion-limited aggregation, DLA, [39] except that the molecules that accrete to an aggregate are often macromolecules rather than monomers, and so the process might be better labelled as cluster–cluster aggregation [40, 41]. This is visualized statically in Fig. 2.8. If the gel point is defined by the stage at which there is a bonded pathway that crosses the simulation space, gelation occurs when two (sometimes three) large clusters react together. These simulations have never observed gelation due to a single growing macromolecule. Macromolecular clusters are more or less reacted material whose surface has only limited remaining functionality with which to react to join a neighboring cluster. Thus, there are intercluster regions or fissures within the final crosslinked mass that are not spanned frequently by chemical bonds and where pendant chains may lie.

Supermolecular nodular structures in crosslinked networks created using a variety of chemistries have been observed and commented on since at least 1959 [42, 43]. Initially, it was natural to suspect that such heterogeneities, of some tens of nanometers in extent, were an experimental artifact; however, that does not appear

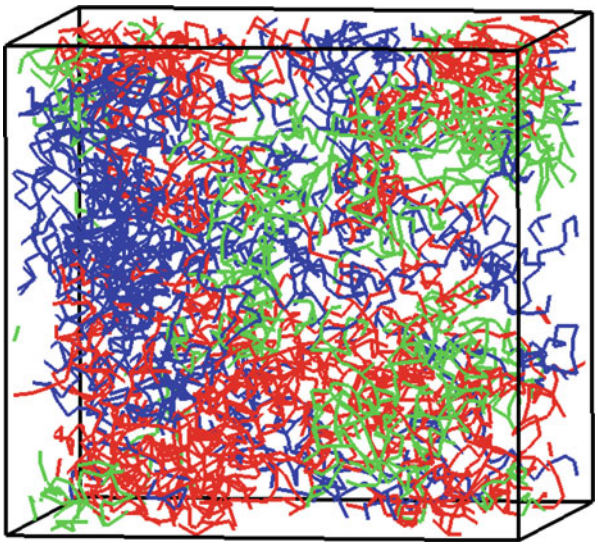

Fig. 2.8 The three largest clusters after crosslinking the 3-functional model for 13,600 time steps. The largest cluster (*red*) contains 2156 nodes, the second largest (*blue*) contains 1992 nodes, and the third largest cluster (*green*) contains 1154 nodes. The total system size is 11,424 nodes. Note the ramified structure of the clusters and the extent to which they are interdigitated. The fractal dimension of the clusters is close to that of percolation clusters

to be the case, since they have been observed a number of times using modern experimental techniques [44, 45]. Our simulation results are consistent with those observations. The center of clusters formed in our coarse-grained simulations would be the denser material seen in observations of such nodular structures. They arise from the growth of the network from a large number of starting points. This is consistent with experimental observations that the nodular heterogeneities form prior to gelation and do not change significantly thereafter [44, 46]. The network formation behavior via cluster aggregation exhibited in the simulations therefore provides a very simple, natural origin for supermolecular heterogeneities, without requiring any particular combination or variation in chemistry. Crosslinked networks do not, and cannot, form homogeneously [47].

Another consequence of the formation of clusters is that spatially neighboring beads may not be bonded together directly. A pendant is a chain of molecules connected to the elastically active network by a single junction. This type of structure is inevitable in randomly crosslinked systems and is caused by the highly ramified structure of pre-gel clusters during crosslinking (see Fig. 2.8). As might be seen in the figure, there are a significant number of linear chains; if these chains do not crosslink to adjacent chains before crosslinking is completed, they occupy a volume across which there are no bonds and which may open up to form a void if the network is subjected to swelling. If these pendants are a number of bonds in length, they will be coiled, at random, so the resulting volumes can be several bond

lengths in size. As will be shown in the following, these voids occur throughout a crosslinked network, and regions of low crosslinking may be very significant in extent, as can be seen in the images published in the experimental investigations mentioned above [42–44, 46, 47].

Swelling and Voids

A crosslinked polymer, when placed in a good solvent, will absorb a portion of the solvent and swell. The extent of swelling is determined by a competition between the free energy of mixing, which will cause the solvent to penetrate and expand the network and an elastic reactive force which opposes this deformation. Since the steady-state swelling ratio is a direct function of the extent of crosslinking, swelling experiments are a simple way to characterize polymer networks. In addition, a molecular intruder will be better able to penetrate where the crosslinking level is low. As they penetrate, the intruding molecules cause the network to swell and thus open up pathways for further intrusion. Allowing a network to swell, after it has been cured, provides a useful and relevant way to visualize and quantify these extensive heterogeneities. These networks were also shown to cavitate if their boundaries were constrained against the shrinkage caused by the crosslinked bonds being shorter than the van der Waals bonds [29]. The tendency to form cavitation voids first brought attention to the possible presence of extended weaknesses in such networks.

The bond potentials along the network backbone provide network integrity, and the attractive tails of the nonbonded van der Waals interactions maintain the system in the high-density condensed state. Instead of swelling by a good solvent, a similar effect can be achieved by replacing the Lennard-Jones nonbonded interactions with a purely repulsive potential obtained by cutting off the LJ potential at its minimum and shifting it upward so that the potential is zero at the cutoff. Thermal fluctuations will then cause the networks to swell until the fluctuation-induced entropic forces are balanced by the network restoring forces. In order to better visualize the larger-scale heterogeneities, the network was allowed to expand in this way and expose any regions of low crosslink density, voids, or other network structures.

As can be seen in Fig. 2.9, which shows the number density of the networks as a function of the number of time steps, the networks swell very quickly at zero load when the attractive tails of the LJ interactions are removed, so this is a rapid, convenient approach.

We present here results only for networks crosslinked at one representative high temperature, $T = 1.0$, and one low temperature, $T = 0.1$. These two cases are sufficient to characterize the behavior in the highly crosslinked networks formed at high temperatures and the more loosely crosslinked systems, with a lower conversion, created at low temperatures. As anticipated, networks for the 3-functional model can expand significantly more than those for the 6-functional model because the length of the chains between junctions is longer (five bond lengths for the

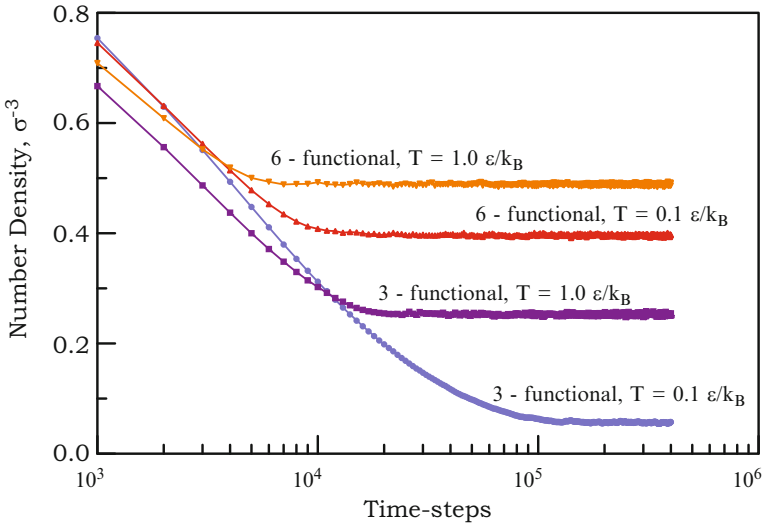

Fig. 2.9 Relaxation of the number densities as a function of the number of time steps for both the 6- and 3-functional networks at $T = 1$ and $T = 0.1$. Initial densities: 0.95 (6-functional, $T = 1$), 1.09 (6-functional, $T = 0.1$); 0.907 (3-functional, $T = 1$), 1.09 (3-functional, $T = 0.1$). The time step is 0.005τ, so the run is of duration 2000τ

3-functional as opposed to three bond lengths for the 6-functional model), and the more tightly crosslinked networks expand less than the networks crosslinked to a lower conversion at low temperatures.

As the network swells, voids open up, the sizes of which depend on the model and the conversion. In the following, we characterize the pore size by the distance, d, from any point to the closest network node on a uniformly spaced $80 \times 80 \times 80$ grid spanning the simulation cell. A distance d^* is chosen as a criterion to distinguish regions of low density from those of more normal density. The volume fraction of a void, such that a node is located a distance greater than d^* from another node, is therefore the number of grid points with separation $d > d^*$ (divided by the volume of the simulation space, 80^3). Isosurfaces are shown in Fig. 2.10 with d^* being the value defining these pore regions. An isosurface is the surface bounding a volume within which the distance to the nearest network node is greater than the chosen value of d^*. Thus, particles with a diameter less than $2d^*$ would be able to diffuse readily through the network inside these isosurfaces. Figure 2.10 shows the network backbone and void isosurfaces for $f = 3$ and $f = 6$ functionality model networks crosslinked at $T = 1$ (left figure) and $T = 0.1$ (right figure). For comparison, bonds in these networks are of approximately unit length. In these visualizations, one can see that the voids, which expand in regions not held together by crosslink bonded forces, are quite large indicating that there are extensive defected regions in these networks. This is true, even in the networks cured at a very high temperature to almost complete conversion at $T = 1$. Even when fully cured, the networks are not ideal and not homogeneous.

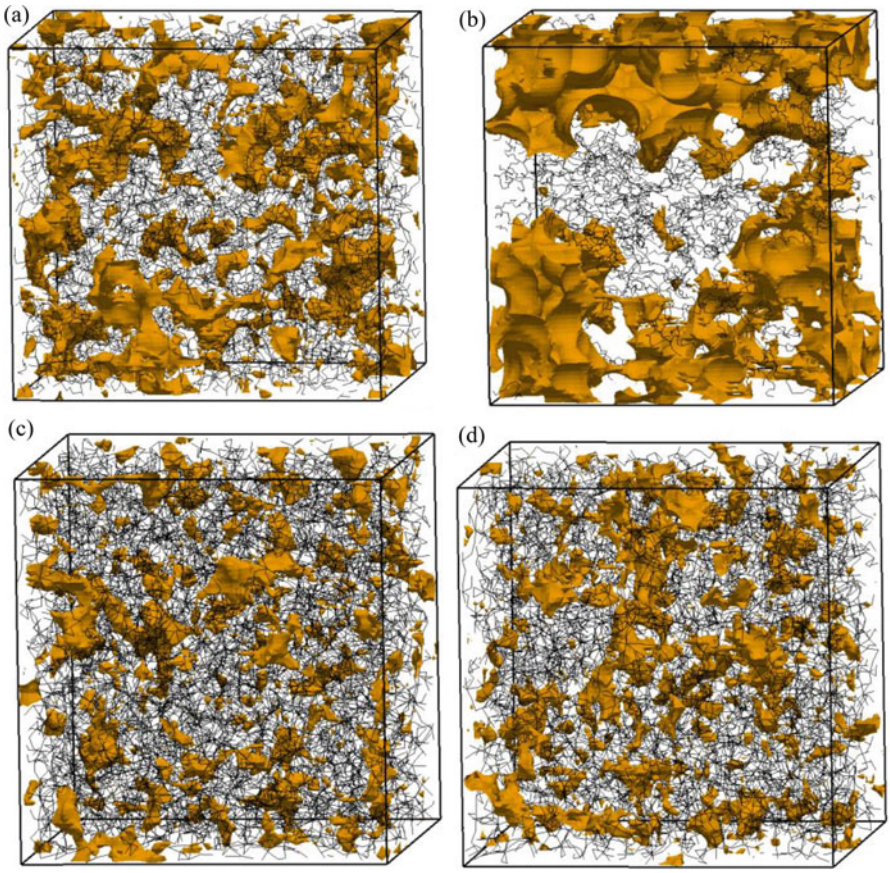

Fig. 2.10 Pore space isosurfaces for expanded networks. The networks were formed first by crosslinking the 3-functional model for 12 million time steps and the 6-functional for 6 million time steps. In each case, the *left figure* was crosslinked and expanded at $T = 1.0$ with isosurfaces for d^* as labelled. The *right-hand side figure* is for $T = 0.1$. The *dark lines* show the network backbones. (**a**) 3-functional, $T = 1.0$, $d^* = 1.8$; (**b**) 3-functional, $T = 0.1$, $d^* = 4$; (**c**) 6-functional, $T = 1.0$, $d^* = 1.3$; (**d**) 6-functional, $T = 0.1$, $d^* = 1.4$

There are obvious and expected qualitative differences. The void extent is more pervasive in the 3-functional system at both temperatures. However, it is striking how many regions of low crosslinking there are even in the 6-functional system that has been cured at a high temperature. By no means can one consider the whole volume or thickness of the material as providing barrier properties or mechanical strength.

The Flory–Rehner calculation of swelling by a solvent [12] assumes that the crosslinked polymer forms an ideal homogeneous network, without significant open voids when swollen, which is not consistent with what we observe. Figure 2.11 gives the volume of the simulation cell of the crosslinked network as a function of

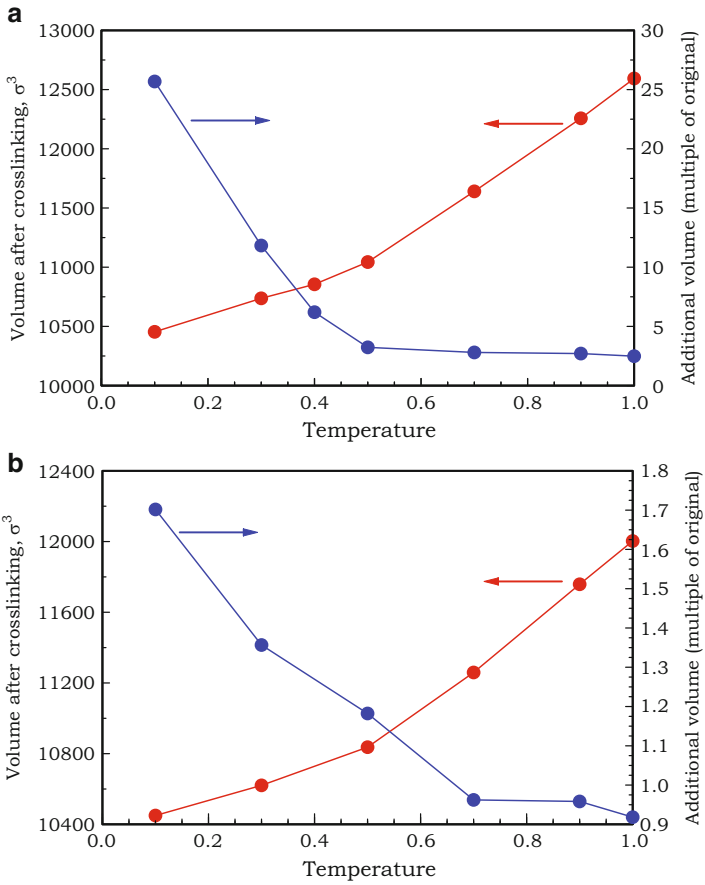

Fig. 2.11 Volume of the simulation cell of the crosslinked network before swelling, V_0, and the volume increase upon expansion, $(V - V_0)/V_0$, where V is the volume after expansion, for the 3-functional (**a**) and 6-functional (**b**) models, as a function of the crosslinking temperature, T

curing temperature, before swelling, V_0, and the reduced volume increase, $(V - V_0)/V_0$, where V is the volume after expansion, for the 3-functional and the 6-functional models. The networks were allowed to expand at the same temperature at which they were crosslinked. Figure 2.12 is a plot of the same data as a function of the conversion. For both models, the cured volume of the system increases with temperature, showing that the entropic contribution to the internal pressure is proportional to T (thermal expansion). On the other hand, the fractional volume change after swelling increases with decreasing temperature, particularly for $T < 0.5$ in the 3-functional model and $T < 0.7$ for the 6-functional model, where the conversion is lower and the networks have fewer saturated junctions. When

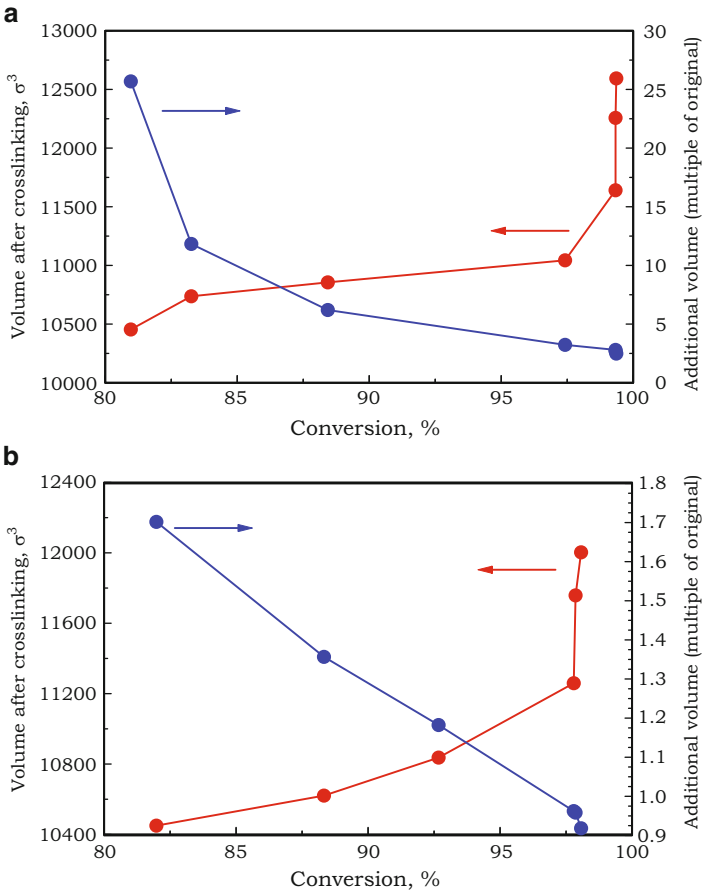

Fig. 2.12 Volume of the simulation cell of the crosslinked network before swelling, V_0, and the volume increase, $(V - V_0)/V_0$, where V is the volume after expansion, for the 3-functional (**a**) and 6-functional (**b**) models, as a function of the final conversion. The same data are used as in Fig. 2.11

expressed as a function of the conversion, the reduced volume change for the 6-functional model increases linearly as the conversion decreases. For the 3-functional model, the increase in the capacity to swell at low conversions is stronger, reflecting the fact that the low conversion networks in this case have conversions only slightly larger than at the gel point, i.e., a conversion of 0.77. The conversion at the gel point for the 6-functional system is 0.557 [29, 34].

Figure 2.13 shows the void volume, as a fraction of the overall expanded network, after the expansion procedure for networks crosslinked at temperatures ranging from $T = 0.1$ to $T = 1.0$, as a function of the choice of d^*. The left panel contains results for the 3-functional model and the right panel for the 6-functional model. Expanded void volumes are much larger for the 3-functional system than for

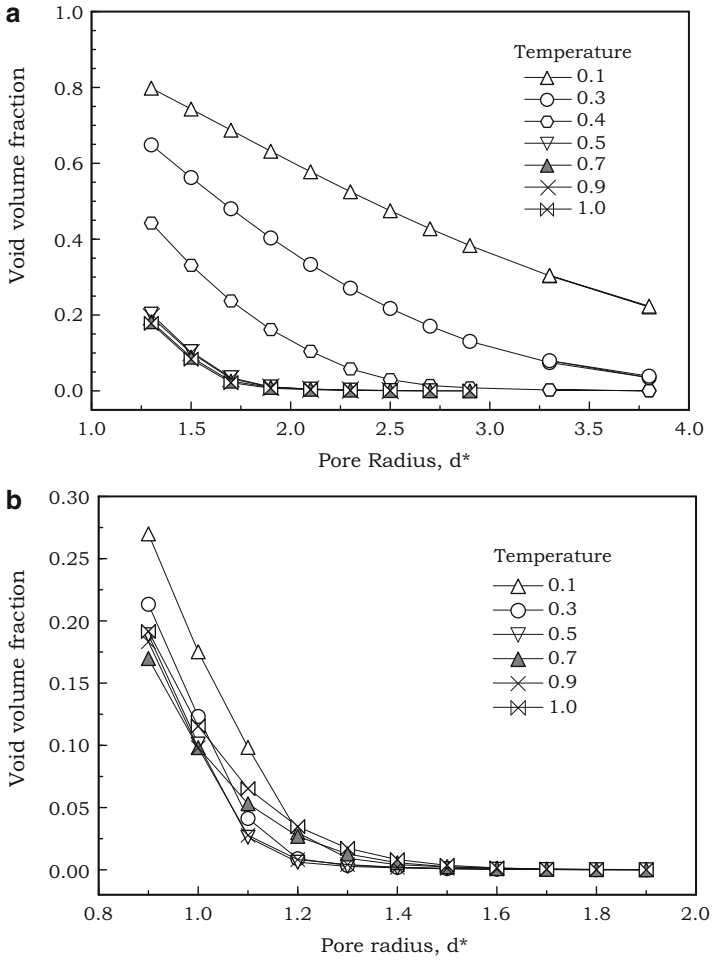

Fig. 2.13 Total void volume for (**a**) the 3-functional and (**b**) the 6-functional models, for different curing temperatures

the more tightly crosslinked 6-functional model, consistent with the longer tails for the 3-functional model in the topological distance distribution function shown in Fig. 2.6 and the larger interjunction separation in the model.

It can be seen in Fig. 2.10 that the voids are seldom spherical in nature but have an extended shape that supports the idea that their origin lies at the intersection of ramified molecular clusters, where pendant chains are more likely. In some cases, if there was some additional network degradation due to weathering, one can see that a percolating pathway might arise fairly readily. If we are interested in gauging whether an intrusive molecule might be able to penetrate the network, then

Fig. 2.13 demonstrates in a quantitative way how the intruder size will affect the outcome. For comparison, a bond is about one unit long in the dimensions of the expanded network. Small penetrating molecules will find many more weaknesses in the network to exploit than would a larger molecule.

Further investigation into the sizes of the nascent voids shows that when the expanded void volume is large, depending on the pore size parameter and the conversion, the vast majority of the pore volume is in the largest pore, with minor contributions from the second and third largest. There are comparatively few extensive voids in the volume simulated here, which is consistent with gelation being the result of two or possibly three molecular clusters dominating the gelation behavior in the simulation volumes here. It is also consistent with the number of cavitation voids formed in these systems under slightly different circumstances [29]. The contribution from the second largest void can be quantified by comparing results plotted in Fig. 2.13 with the corresponding data for the second largest void in Fig. 2.14.

As the pore size parameter, d^*, is increased, the size of the largest nascent pore decreases, and the size of the second (as well as third and higher) nascent pores increases to a peak before decreasing again for larger d^*. The position of this peak lies at slightly larger d^* than the value at which the largest pore would no longer percolate across the system. A similar relationship between the position of the peak in the size of the second largest cluster and the location of the gel point in the model systems used here has been noted before [48].

For the current models and system size used here, the largest pore percolates when its volume is on the order of 4% of the system size, a value which is attained in the 3-functional model for a pore radius in the range 1.5–1.6. For the 6-functional model, a smaller d^* is required, on the order of 1.0–1.1; even then, however, the diameter of the pore is significantly larger than the bead diameter in our models.

These results demonstrate that extensive heterogeneities, exposed as nascent voids, can occur throughout a crosslinked network and may occupy a significant fraction of the volume if it is swollen by fluctuations, as here, or in practice, by a solvent or internal stress. While normally closed because of the attractive van der Waals forces between network components, these regions can facilitate the passage of a penetrant molecule, or be the locus of a fracture surface, even before degradation. These weak regions are where an external molecule would have the best opportunity to penetrate and thus swell the network, opening it up further. The important point is that it was only the random fluctuations intrinsic to the crosslinking process that produced these regions not held together by bonded forces. There is no equivalent to a Maxwell demon that ensures that an ideal network is formed everywhere.

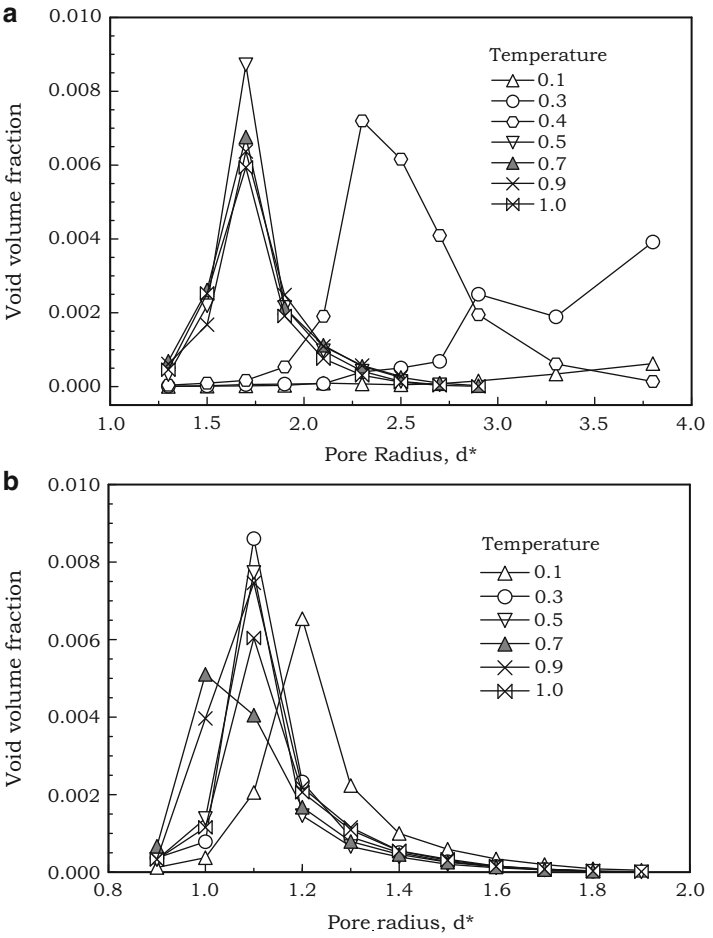

Fig. 2.14 Volume fraction of second largest pore (**a**) 3-functional system, (**b**) 6-functional system, for different curing temperatures

Summary

Modern computers provide the opportunity to analyze in detail the structure of networks and learn more about how crosslinked polymer networks form. Although it had been realized from the start that randomly crosslinked networks would contain dangling ends and loops, as well as other topological defects, which would diminish anticipated performance, predictive theories based on statistical approaches necessarily assumed that the eventual network was perfect and homogeneous in the sense that all reactive species would combine as expected. Molecular dynamic simulations show how the random nature of the crosslinking process involving huge numbers of small molecules inevitably produces nonideal, defected networks.

In terms of mechanical properties, the effect of those features that diminish the number of elastically effective network chains and junctions can be quantified by comparison between simulation results and the predictions for ideal networks given by the Miller–Macosko approach. In this case, the primary deviation from ideality is the formation of primary loops. In particular, network junctions in the 6-functional system have approximately a 75% chance of having a primary loop occupying two of its reactive sites at conversions close to 100%. At lower conversions, the number of primary loops decreases rapidly, and agreement with Miller–Macosko calculations is better. In contrast, simulations of the 3-functional system indicate that it is much less sensitive to the curing temperature. There is a smaller reduction in the absolute number of elastically effective crosslink chains and cycle rank, and the ratio of these parameters remains close to predictions for an ideal network. In this case, fewer loops can form after one functionality on a crosslinker has reacted with one end of a dimer because, for the other end of the dimer, there are only two sites on that crosslinker remaining to compete with unreacted sites on neighboring crosslinkers. In either case, a lower curing temperature might permit a more ideally formed network, but this may not be practical due to the very much longer curing time that would be necessary to achieve high conversion and thus good properties. Although cycle rank was introduced as a quantity for characterizing networks based on the number of elastically active, complete loops, any predictive calculation assumes that the network is ideal and thus must be an overestimate. These loops and unreacted groups are defects that are comparable in size to the initial precursor molecules.

Other imperfections occur that are more extensive in nature. Simulations show that polymer networks form by the aggregation of ramified cluster-like macromolecules, resulting in networks with a significant number of topological defects and heterogeneities. These clusters that form largely prior to gelation provide a natural explanation for the formation of nodular structures, or phase differences, seen experimentally, but where the explanation is derived more from the statistical nature of network formation rather than any combination of chemistry. Due to mobility restrictions and prior reactions, the surfaces of the erstwhile clusters are regions where there will be a reduced chance of a bond forming a link to a neighboring cluster or a long pendant chain remaining unreacted. These regions, where there are a reduced number of crosslinks to junctions in close spatial proximity, can extend over a significant fraction of the simulation cell and thus may join to form percolating pathways where external penetrating molecules could find a route to attack the substrate that the coating is protecting. The heterogeneous, nodular structure must diminish the mechanical properties compared to the potential in a perfectly homogeneous material. The number and type of defects depend on the crosslinker functionality, the length of the primary chains between crosslinkers, as well as the final conversion and crosslinking temperature. These features will have a scale comparable to the extent of the macromolecular clusters at the gelation point.

The extent of these intercluster fissures can be visualized by diminishing the LJ (van der Waals) forces between the beads after the simulation has formed the

network. The resultant expansion of the network, and analysis of the void structure that appears where these defects occurred, provides information about the size and distribution of these extensive regions of low crosslinking. In any real polymer network, these fissures would be of the order of nanometers or tens of nanometers in size, so they are not large enough to initiate fracture themselves, but they could be the starting point for subsequent damage to grow and limit the ultimate strength of the material. It is also easy to appreciate the size of molecule that may be able to intrude and contribute to a variety of failure modes. The solvent swelling of a network is likely, in some cases, to be significantly more than that described by the Flory–Rehner and related models because of the potential for extensive voids that could form in the intercluster regions.

Regardless of the model details, networks contain defects of a small local nature and defects that are more extensive where the network is not held together by chemical bonds. These regions open up to form voids when the network is swelled or exposed to other stresses. While the systems examined here cannot represent all possible precursor combinations, we expect that the features we describe are typical of most types of resultant networks.

Acknowledgements The authors are glad to acknowledge computer access, financial, and administrative support from the North Dakota State University Center for Computationally Assisted Science and Technology and the U.S. Department of Energy through Grant No. DESC0001717.

References

1. Flory, P.J.: Network structure and the elastic properties of vulcanized rubber. Chem. Rev. **135**, 51–75 (1944)
2. Flory, P.J.: Principles of Polymer Chemistry. Cornell University Press, Ithaca (1953)
3. Stockmayer, W.H.: Theory of molecular size distribution and gel formation in branched-chain polymers. J. Chem. Phys. **11**(2), 45–55 (1943)
4. Stockmayer, W.H.: Theory of molecular size distribution and gel formation in branched polymers II. General cross linking. J. Chem. Phys. **12**(40), 125–131 (1944)
5. Dušek, K.: Crosslinking and networks. Makromol. Chem. Suppl. **2**, 35–49 (1979)
6. Cail, J.I., Stepto, R.F.T.: The gel point and network formation—theory and experiment. Polym. Bull. **58**(1), 15–25 (2007)
7. Zhou, H., Woo, J., Cok, A.M., Wang, M., Olsen, B.D., Johnson, J.A.: Counting primary loops in polymer gels. Proc. Natl. Acad. Sci. USA. **109**(47), 19119–19124 (2012)
8. Duering, E.R., Kremer, K., Grest, G.S.: Structure and relaxation of end-linked polymer networks. J. Chem. Phys. **101**, 8169–8192 (1994)
9. Duering, E.R., Kremer, K., Grest, G.S.: Structural properties of randomly crosslinked polymer networks. Progr. Colloid Polym. Sci. **90**, 13–15 (1992)
10. Gordon, M.: Good's theory of cascade processes applied to the statistics of polymer distributions. Proc. R. Soc. Lond. A Math. Phys. Sci. **268**, 240–256 (1962)
11. Treloar, L.R.G.: The Physics of Rubber Elasticity. Clarendon Press, Oxford (1958)
12. Flory, P.J., Rehner, J.: Statistical mechanics of swelling of crosslinked polymer networks. Chem. Phys. **11**, 521–526 (1943)

13. Coniglio, A., Stanley, H.E., Klein, W.: Site-bond correlated-percolation problem: a statistical mechanical model of polymer gelation. Phys. Rev. Lett. **42**(8), 513–522 (1979)
14. Gujrati, P.D.: Thermal and percolative transitions and the need for independent symmetry breakings in branched polymers on a Bethe lattice. J. Chem. Phys. **98**(2), 1613–1634 (1993)
15. Dušek, K.: My fifty years with polymer gels and networks and beyond. Polym. Bull. **58**, 321–338 (2007)
16. Dušek, K., Dušková-Smrčková, M.: Network structure formation during crosslinking of organic coating systems. Prog. Polym. Sci. **25**, 1215–1260 (2000)
17. Dušek, K., Dušková-Smrčková, M., Huybrechts, J., Ďuračková, A.: Polymer networks from preformed precursors having molecular weight and group reactivity distributions. Theory and application. Macromolecules. **46**, 2767–2784 (2013)
18. Miller, D.R., Macosko, C.W.: Molecular weight relations for crosslinking of chains with length and site distribution. J. Polym. Sci. B Polym. Phys. **25**, 2441–2469 (1987)
19. Miller, D.R., Macosko, C.W.: Network parameters for crosslinking of chains with length and site distribution. J. Polym. Sci. B Polym. Phys. **26**, 1–54 (1988)
20. Dušek, K., Spěváček, J.: Cyclization in vinyl–divinyl copolymerization. Polymer. **21**, 750–756 (1980)
21. Tiemersma-Thoone, G.P.J.M., Scholtens, B.J.R., Dušek, K., Gordon, M.: Theories for network formation in multistage processes. J. Polym. Sci. B Polym. Phys. **29**, 463–482 (1991)
22. Flory, P.J.: Statistical thermodynamics of random networks. Proc. R. Soc. Lond. A Math. Phys. Sci. **351**, 351–380 (1976)
23. Queslel, J.P., Mark, J.E.: Molecular interpretation of the moduli of elastomeric polymer networks of known structure. Adv. Polym. Sci. **85**, 135–176 (1984)
24. Flory, P.J.: Elastic activity of imperfect networks. Macromolecules. **15**, 99–100 (1982)
25. Grest, G.S., Kremer, K.: Statistical properties of random cross-linked rubbers. Macromolecules. **23**, 4994–5000 (1990)
26. Stevens, M.J.: Interfacial fracture between highly cross-linked polymer networks and a solid surface: effect of interfacial bond density. Macromolecules. **34**, 2710–2718 (2001)
27. Tsige, M., Stevens, M.J.: Effect of cross-linker functionality on the adhesion of highly crosslinked polymer networks: a molecular dynamics study of epoxies. Macromolecules. **37**, 630–637 (2004)
28. Tsige, M., Lorenz, C.D., Stevens, M.J.: Role of network connectivity on the mechanical properties of highly cross-linked polymers. Macromolecules. **37**, 8466–8472 (2004)
29. Zee, M., Feickert, A.J., Kroll, D.M., Croll, S.G.: Cavitation in crosslinked polymers: molecular dynamics simulations of network formation. Prog. Org. Coat. **83**, 55–63 (2015)
30. Plimpton, S.: Fast parallel algorithms for short-range molecular dynamics. J. Comput. Phys. **117**, 1–19 (1995)
31. Pascault, J.-P., Sautereau, H., Verdu, J., Williams, R.J.J.: Thermosetting Polymers. Marcel Dekker, New York (2002)
32. Gillham, J.K.: Formation and properties of thermosetting and high Tg polymeric materials. Polym. Eng. Sci. **26**(20), 1429–1433 (1986)
33. Herrmann, H.J., Hong, D.C., Stanley, H.E.: Backbone and elastic backbone of percolation clusters obtained by the new method of 'burning'. J. Phys. A Math. Gen. **17**, L261–L266 (1984)
34. Kroll, D.M., Croll, S.G.: Influence of crosslinking functionality, temperature and conversion on heterogeneities in polymer networks. Polymer. **79**, 82–90 (2015)
35. Martin, M.G.: MCCCS Towhee: a tool for Monte Carlo molecular simulation. Mol. Simul. **39** (14–15), 1212–1222 (2013)
36. Smit, B.: Phase diagrams of Lennard-Jones fluids. J. Chem. Phys. **96**, 8639–8640 (1992)
37. Ge, J., Wu, G.-W., Todd, B.D., Sadus, R.J.: Equilibrium and nonequilibrium molecular dynamics methods for determining solid–liquid phase coexistence at equilibrium. J. Chem. Phys. **119**, 11017–11023 (2003)

38. Ahmed, A., Sadus, R.J.: Effect of potential truncations and shifts on the solid liquid phase coexistence of Lennard-Jones fluids. J. Chem. Phys. **133**, 124515 (2010)
39. Witten, T.A., Sander, L.M.: Diffusion-limited aggregation. Phys. Rev. B. **27**(9), 5686–5697 (1983)
40. Meakin, P.: Diffusion-limited aggregation in three dimensions: results from a new cluster–cluster aggregation model. J. Colloid Interface Sci. **102**(2), 491–504 (1984)
41. Heinson, W.R., Chakrabarti, A., Sorensen, C.M.: Divine proportion shape invariance of diffusion limited cluster–cluster aggregates. Aerosol Sci. Technol. **49**(9), 786–792 (2015)
42. Erath, E.H., Spurr, R.A.: Occurrence of globular formations in thermosetting resins. J. Polym. Sci. **35**(129), 391–399 (1959)
43. Racich, J.L., Koutsky, J.A.: Nodular structure in epoxy resins. J. Appl. Polym. Sci. **20**(8), 2111–2129 (1976)
44. Morsch, S., Liu, Y., Lyon, S.B., Gibbon, S.R.: Insights into epoxy network nanostructural heterogeneity using AFM-IR. ACS Appl. Mater. Interfaces. **8**, 959–966 (2016)
45. Sahagun, C.M., Morgan, S.E.: Thermal control of nanostructure and molecular network development in epoxy-amine thermosets. ACS Appl. Mater. Interfaces. **4**, 564–572 (2012)
46. Cuthrell, R.E.: Epoxy polymers II. Macrostructure. J. Appl. Polym. Sci. **12**(6), 1263–1278 (1968)
47. Labana, S.S., Newman, S., Chompff, A.J.: Chemical effects on the ultimate properties of polymer networks in the glassy state. In: Chompff, A.J., Newman, S. (eds.) Polymer Networks, pp. 453–477. New York, Plenum Press (1971)
48. Zee, M.: Structures of crosslinked networks. Master's thesis, North Dakota State University. ProQuest Dissertations Publishing, 1589686 (2015)

http://www.springer.com/978-3-319-51625-7

Protective Coatings
Film Formation and Properties
Wen, M.; Dušek, K. (Eds.)
2017, VIII, 510 p. 271 illus., 136 illus. in color.,
Hardcover
ISBN: 978-3-319-51625-7